JOURNAL OF GUIDANCE, CONTROL, AND DYNAMICS
Vol. 30, No. 4, July–August 2007

Relative Motion Control for Autonomous Rendezvous Based on Classical Orbit Element Differences

Chen Tong* and Xu Shijie†
Beihang University, Beijing 100083, People's Republic of China
and
Wang Songxia‡
University of Nottingham, Nottingham, NG7 2RD England, United Kingdom

DOI: 10.2514/1.28250

Relative motion control strategies for autonomous rendezvous operations in a near-circular orbit are presented in this paper. The relative motion equations described by classical orbit element differences are adopted and the periodic drift in along-track motion is deduced from the along-track motion equation. The control strategies in two different measurement cases are designed based on the periodic characteristics of relative motion. In the first case, the measurements of relative range and line-of-sight angles are available to estimate the relative position and velocity. The three-axis impulsive control strategies to adjust along-track, radial, and cross-track motions are designed using Gauss's perturbation equations. In the second case, only line-of-sight angles are available. An iterative algorithm is presented to estimate the along-track motion using only the azimuth angle to obtain the impulsive changes to adjust the along-track motion. Numerical simulations are undertaken to verify the control strategies proposed. The results indicate that 1) three-axis motions can be controlled accurately when the relative range and line-of-sight angles are available and 2) the iterative algorithm is valid for along-track drift control when only line-of-sight angles are available.

Nomenclature

A_y	=	amplitude of the cross-track motion
A_z^{des}	=	desired amplitude of the radial motion
a	=	semimajor axis
a_c	=	semimajor axis of the chaser
a_t	=	semimajor axis of the target
D_{des}	=	desired drift of the along-track motion within each period
e	=	eccentricity
e_c	=	eccentricity of the chaser
e_t	=	eccentricity of the target
f_h	=	component of the control acceleration along the orbital angular momentum vector
f_n	=	component of the control acceleration perpendicular to the velocity vector
f_t	=	component of the control acceleration along the velocity vector
f_x	=	component of the control acceleration in the along-track motion
f_y	=	component of the control acceleration in the cross-track motion
f_z	=	component of the control acceleration in the radial motion
h	=	massless angular momentum of orbital motion
i	=	orbit inclination
i_c	=	orbit inclination of the chaser
i_t	=	orbit inclination of the target
M	=	mean anomaly
M_c	=	mean anomaly of the chaser
M_t	=	mean anomaly of the target
P	=	orbit period
P_c	=	orbit period of the chaser
P_t	=	orbit period of the target
$\boldsymbol{r}_c$	=	position vector of the chaser
$\boldsymbol{r}_t$	=	position vector of the target
t_p	=	time of passing perigee
t_{pc}	=	time of passing perigee of the chaser
t_{pt}	=	time of passing perigee of the target
u	=	argument of latitude
u_c	=	argument of latitude of the chaser
u_t	=	argument of latitude of the target
v	=	velocity of the spacecraft
x	=	along-track component of relative position in the chaser local vertical, local horizontal frame
y	=	cross-track component of relative position in the chaser local vertical, local horizontal frame
z	=	radial component of the relative position in the chaser local vertical, local horizontal frame
$z_{\max}$	=	maximum radial motion in a target orbit period
$z_{\min}$	=	minimum radial motion in a target orbit period
β	=	phrase angle of the relative orbit
Δa_{des}	=	desired value of the semimajor axis difference
$\lvert\Delta e\rvert_{\text{des}}$	=	desired amplitude of the eccentricity difference
Δi_{des}	=	desired values of the orbit-inclination difference
Δv_y	=	cross-track impulsive velocity change
Δv_x^a	=	impulsive velocity change required to adjust the semimajor axis
Δv_z^e	=	impulsive velocity change required to adjust the eccentricity
Δv_y^i	=	cross-track impulsive velocity change required to adjust the orbit inclination
Δv_y^Ω	=	cross-track impulsive velocity change required to adjust the right ascension node
$\Delta\Omega_{\text{des}}$	=	desired values of the right-ascension-node difference
δa	=	desired corrections of the semimajor axis of the chaser

Received 12 October 2006; revision received 15 March 2007; accepted for publication 16 March 2007.

*Ph.D. Student, Spacecraft Dynamics and Control, School of Astronautics, Laboratory 504, Haidian District; astrochet1980@hotmail.com.

†Professor, Spacecraft Dynamics and Control, School of Astronautics, Laboratory 504, Haidian District.

‡Ph.D. Student, Global Positioning System Navigation, University of Park Campus, Institute of Engineering Surveying and Space Geodesy; isxsw@nottingham.ac.uk.

δe = desired corrections of the eccentricity of the chaser
δi = desired corrections of the orbit inclination of the chaser
$\delta\Omega$ = desired corrections of the right ascension node of the chaser
θ = true anomaly
θ_c = true anomaly of the chaser
θ_t = true anomaly of the target
θ_y = azimuth
θ_z = elevation
μ = gravitational constant of Earth
ν_r = relative range measurement noise
ν_y = azimuth measurement noise
ν_z = elevation measurement noise
$\boldsymbol{\rho}$ = position vector of the target relative to the chaser
σ_{px} = standard deviation of along-track random acceleration
σ_{py} = standard deviation of cross-track random acceleration
σ_{pz} = standard deviation of radial random acceleration
σ_r = standard deviation of relative range measurement noise
σ_y = standard deviation of azimuth measurement noise
σ_z = standard deviation of elevation measurement noise
ς_x = along-track random acceleration
ς_y = cross-track random acceleration
ς_z = radial random acceleration
Ω = right ascension node
Ω_c = right ascension node of the chaser
Ω_t = right ascension node of the target
ω = argument of perigee
ω_c = argument of perigee of the chaser
ω_t = argument of perigee of the target
ϖ_c = angular velocity of the chaser

Introduction

IN RECENT years, there has been increasing interest in autonomous rendezvous technology, following several decades of development [1–4]. As mentioned in [2], the autonomous rendezvous mission can be divided into several different phases, according to the relative distance between the two spacecraft and the source of navigation data. Each phase requires different methods for relative navigation and relative motion control. Therefore, the relative navigation and the dynamics and control of relative motion are two key technologies for autonomous rendezvous.

The relative navigation that supplies measurements for relative motion control is closely related to the sensors and the characteristics of measured targets. With a cooperative target, satisfactory sensors and global positioning system (GPS) receivers, it is simple to supply sufficient measurements: relative range, azimuth and elevation angles, and inertial positions and velocities of spacecraft. But with a noncooperative target, insufficient or disabled sensors, and without GPS receivers, the relative navigation and relative motion control are usually extraordinarily difficult because of insufficient data. Hablani et al. [5,6] summarized and developed relative navigation algorithms for many cases. Significantly, observability of the relative position from angle measurements was examined in [6]. Crassidis et al. [7,8] also discussed this problem; they almost came to the same conclusion that the relative position is unobservable using only line-of-sight (LOS) angles measurements in the local vertical, local horizonal (LVLH) frame. Although, using a Kalman filter, the relative position has been estimated with only LOS angles available in [6], the results were rough and the errors were too large to design maneuver strategies for autonomous rendezvous. However, in the relative drift phase (from several kilometers to hundreds of kilometers) of autonomous rendezvous, only LOS angles measurements may be available, because of insufficient sensors. Therefore, it is necessary to study relative navigation and relative motion control with only LOS angles available. In general, the relative navigation and the configuration and status of sensors for measurement are critical to mission success, because they determine whether the acquirable information is enough to implement relative motion control.

The studies of relative motion of spacecraft began in the 1960s with the paper by Clohessy and Wiltshire (C-W equations) [9], who derived the equations of motion for one spacecraft relative to another that is in a circular orbit about spherical Earth. The C-W equations are also called Hill's equations, which were obtained by Hill using the same method in the research about the moon [10]. Based on the C-W equations, many guidance algorithms were developed for rendezvous operations [11–17]. The R-bar, V-bar, and Lambert transfer are the most common algorithms for approach or retirement operations (see [9]). Prussing [12,13] and Carter [14] investigated minimum-propellant impulsive-rendezvous maneuvers using optimal control theory. Lopez and McInnes [15] presented artificial potential function guidance algorithms for terminal rendezvous in the presence of path constraints and multiple obstructions. Lovell and Tragesser [16,17] transformed the C-W coordinates to a new set of parameters, termed relative orbit elements, that give a clear representation of the geometry of the relative motion and investigated guidance algorithms. However, it is acknowledged that the C-W equations are not accurate enough for long-range and long-term relative motion control because of the linearization error, the eccentricity error, the perturbative effect of J_2, and so on. Therefore, the relative motion in an elliptic orbit was studied [18–23]. Furthermore, with the formation flying concept presented, more accurate models (including high-order terms, the eccentricity, and the J_2 perturbation) were developed [24–28]. Schaub and Alfriend [29–31] and Schaub [32] presented an innovative method to describe the relative motion in terms of classical orbit element differences. Meanwhile, several relative motion control strategies that feed back classical orbit element differences have been suggested for formation flying [33,34]. It is extraordinarily advantageous to analyze the long-term characteristics of relative motion using classical orbit element differences. Another advantage of this method is that relative motion control strategies can be designed using classical Gauss's perturbation equations. However, the preceding methods mainly address formation flying tasks and the implementations of control strategies require abundant measurements including the inertial measurements of the spacecraft, some of which are likely unavailable in missions with insufficient sensors. As is known, there are no reported works for autonomous rendezvous operations based on classical orbit element differences. Therefore, it is necessary to attempt to develop control strategies based on classical orbit element differences for autonomous rendezvous.

In this paper, we present relative motion control strategies based on classical orbit element differences for the relative drift phase of autonomous rendezvous in a near-circular orbit with only relative measurements available, but not any inertial measurements. Especially, an iterative algorithm is presented for drift control when only LOS angles are measured, but not the relative range. This paper is organized as follows: First, based on the approaches in [29,30], the relative motion equations in the chaser LVLH coordinate system are established. Then the periodic characteristics of relative motion are investigated, and the relation between the along-track motion and the semimajor axis differences is developed. Next, the relative motion control strategies are designed when the relative position and relative velocity are acquired. The three-axis control strategies are given with impulsive changes. Afterwards, the impulsive control strategy for along-track motion using only the azimuth angle is presented. Finally, these control strategies are illustrated with two numerical simulation scenarios.

Relative Motion Equations Expressed in Classical Orbit Element Differences

As seen in Fig. 1, the LVLH frame origin is at the center of mass of the chaser spacecraft, the X axis lies in the orbit plane and perpendicular to the position vector $\boldsymbol{r}_c$ of the chaser (pointing forward), the Z axis points to the center of mass of the earth, and the Y axis is normal to the orbit plane and forms a right-handed set with the X and Z axes. In the chaser LVLH coordinate system, the relative position vector of the target with respect to the chaser is defined as $\boldsymbol{\rho} = [x\ y\ z]^T$.

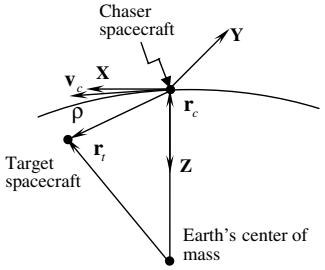

Fig. 1 Scenario 1: LVLH frame centered on the center of mass of the chaser spacecraft.

In general, relative motion equations describe the relative motion of the chaser with respect to the target in the target LVLH frame. But in autonomous rendezvous, the measurement information is always about the target with respect to the chaser in the chaser frame. In this paper, to analyze the relative motion using the measurement information directly and to obtain the guidance signals in the chaser frame, the relative motion equations of the target with respect to the chaser are described in the chaser LVLH frame in terms of the classical orbit element differences.

The relative motion equations in the chaser LVLH frame are established based on the works of [29,30]. The orbit elements are defined as follows: the semimajor axis, the eccentricity, the right ascension node, the orbit inclination, the argument of perigee, the true anomaly, the argument of latitude ($u = \omega + \theta$), the mean anomaly, the time of passing perigee, and the orbit period. The classical orbit element differences are given by

$$\Delta a = a_t - a_c, \quad \Delta e = e_t - e_c, \quad \Delta\Omega = \Omega_t - \Omega_c$$
$$\Delta i = i_t - i_c, \quad \Delta\omega = \omega_t - \omega_c \quad \Delta\theta = \theta_t - \theta_c$$
$$\Delta u = u_t - u_c, \quad \Delta M = M_t - M_c, \quad \Delta t_p = t_{\mathrm{pt}} - t_{\mathrm{pc}}$$
$$\Delta P = P_t - P_c$$

where the subscripts t and c refer to the target and the chaser, respectively.

The position vector of the target relative to the chaser $\boldsymbol{\rho}$ is

$$\boldsymbol{\rho} = \mathbf{r}_t - \mathbf{r}_c \tag{1}$$

Equation (1) is expanded in the chaser LVLH frame as

$$\begin{bmatrix} x \\ y \\ z \end{bmatrix} = L_{ci}(\Omega_c, i_c, u_c) L_{it}(\Omega_t, i_t, u_t) \begin{bmatrix} 0 \\ 0 \\ -r_t \end{bmatrix} - \begin{bmatrix} 0 \\ 0 \\ -r_c \end{bmatrix} \tag{2}$$

where $L_{ci}(\Omega_c, i_c, u_c)$ is the transformation matrix from the inertial frame to the chaser LVLH frame, $L_{it}(\Omega_t, i_t, u_t)$ is the transformation matrix from the target LVLH frame to the inertial frame, $[0\ 0\ -r_t]^T$ is the column matrix of components of $\boldsymbol{r}_t$ in the target LVLH frame, and $[0\ 0\ -r_c]^T$ is the column matrix of components of $\boldsymbol{r}_c$ in the chaser LVLH frame.

When the relative orbit radius ρ is small in comparison with the absolute orbit radius, the orbit element differences $\Delta\Omega$, Δi, and Δu are small enough to ignore the higher-order small quantities. Equation (2) can then be written as (also see [35])

$$\begin{bmatrix} x \\ y \\ z \end{bmatrix} = \begin{bmatrix} r_t(\Delta u + \Delta\Omega \cos i_t) \\ r_t(\Delta\Omega \sin i_t \cos u_t - \Delta i \sin u_t) \\ r_c - r_t \end{bmatrix} \tag{3}$$

The true anomaly and the spacecraft position can be expressed as the series expansion about Bessel functions [36]. In the case of a near-circular orbit, the second-order and higher-order terms containing eccentricity are negligible and the expressions of the true anomaly and the spacecraft position are simplified as follows:

$$\begin{cases} \theta_c \approx M_c + 2e_c \sin M_c \\ \theta_t \approx M_t + 2e_t \sin M_t \end{cases} \tag{4}$$

$$\begin{cases} r_c \approx a_c(1 - e_c \cos M_c) \\ r_t \approx a_t(1 - e_t \cos M_t) \end{cases} \tag{5}$$

The mean anomalies are expressed as follows:

$$\begin{cases} M_c = 2\pi(t - t_{\mathrm{pc}})/P_c \\ M_t = 2\pi(t - t_{\mathrm{pt}})/P_t \end{cases} \tag{6}$$

After substituting Eqs. (4–6) into Eq. (3) and ignoring terms containing eccentricity and negligible second-order small quantities, the relative motion for a near-circular orbit case is expressed as

$$x = a_t(\Delta\omega - 2\pi t_{\mathrm{pt}}/P_t + 2\pi t_{\mathrm{pc}}/P_c + 2\Delta e \sin M_t + \Delta\Omega \cos i_t) - 2\pi a_t \Delta P t/(P_t P_c) \tag{7a}$$

$$y = a_t\sqrt{\Delta\Omega^2 \sin^2 i_t + \Delta i^2}\,\sin(\beta - u_t) \tag{7b}$$

$$z = -\Delta a + a_t \Delta e \cos M_t \tag{7c}$$

where the phase angle β is defined as

$$\beta = \arctan 2(\Delta\Omega \sin i_t, \Delta i) \tag{8}$$

When the semimajor axes are equal, namely,

$$a_c = a_t = a, \qquad P_c = P_t = P$$

Equation (7) becomes

$$x = a(\Delta\omega - 2\pi\Delta t_p/P + 2\Delta e \sin M_t + \Delta\Omega \cos i_t) \tag{9a}$$

$$y = a\sqrt{\Delta\Omega^2 \sin^2 i_t + \Delta i^2}\,\sin(\beta - u_t) \tag{9b}$$

$$z = a\Delta e \cos M_t \tag{9c}$$

Equations (7) and (9) describe the nonperturbed relative motion for a near-circular orbit case.

Equation (7a) shows that a secular drift term exists in the along-track motion x because of the semimajor axis difference. After one orbit period of the target, the along-track drift quantity is

$$\Delta x_P = -2\pi a_t \Delta P P_t/(P_t P_c) = -2\pi a_t[\sqrt{(a_t/a_c)^3} - 1] \tag{10}$$

With the assumption of a small difference in the semimajor axis, the first-order approximation of Eq. (10) is

$$\Delta x_P = -3\pi\Delta a \tag{11}$$

Equation (11) provides an approximation about how the along-track motion x will vary due to the semimajor axis difference Δa after one orbit period. It is fundamental to the relative motion control in the next sections. Equations (7b) and (7c) show that the cross-track motion y and the radial motion z are periodic motions, with the period equal to the orbit period P_t of the target. The amplitude of cross-track motion y is $a_t\sqrt{\Delta\Omega^2 \sin^2 i_t + \Delta i^2}$.

Equation (9) shows that the relative motion is periodic, with the period equal to the orbit period P_t of the target when the semimajor axes of the spacecraft are equal. The trajectory of relative motion in the X–Z plane is an ellipse with a center at ($a\Delta\omega - 2\pi a\Delta t_p/P + a\Delta\Omega \cos i_t$, 0) and with a semimajor axis $2a|\Delta e|$ along the X axis twice as large as the semiminor axis along the Z axis.

Relative Motion Control Using Measurements of Relative Range and LOS Angles

This section investigates relative motion control under the assumption that the range and LOS angles of the target relative to the chaser can be measured. The relative range measurements are provided by lidar and LOS angles measurements are obtained from cameras and visible or infrared sensors. In this case, the relative position and the relative velocity can be estimated using an extended Kalman filter (EKF) (see [5]), but the real-time orbit elements of the spacecraft cannot be estimated because any inertial measurement is unavailable. The implementation of the algorithm requires the relative position, the relative velocity, and the semimajor axis a_t of the target (regarded as a constant). The three-axis control strategies will be given with impulsive changes.

Along-Track and Radial Control Strategies

In the course of autonomous rendezvous, maneuver operations of approach, retirement, and stationkeeping are necessary. We can control the along-track and the radial motions of the chaser to carry out these operations.

Equation (11) shows that the long-term along-track motion depends on the semimajor axis difference Δa. Equations (7c) and (9c) show that the amplitude of radial motion depends on the magnitude of eccentricity difference $|\Delta e|$. The semimajor axis difference Δa and the magnitude of eccentricity difference $|\Delta e|$ are determined from

$$\Delta a = [x(t + P_t) - x(t)]/(-3\pi) \tag{12}$$

$$|\Delta e| = (z_{\max} - z_{\min})/(2a_t) \tag{13}$$

where P_t is equal to $2\pi\sqrt{a_t^3/\mu}$, time t is arbitrary, and $z_{\max}$ and $z_{\min}$ are the maximum and minimum of radial motion z within one orbit period P_t of the target. Note that the maneuver control is forbidden during the period of determining Δa and $|\Delta e|$.

If the desired drift of along-track motion within each period is D_{des} and the desired amplitude of radial motion is A_z^{des}, the desired value of semimajor axis difference and the desired magnitude of eccentricity difference are given by

$$\Delta a_{\text{des}} = D_{\text{des}}/(-3\pi) \tag{14}$$

$$|\Delta e|_{\text{des}} = A_z^{\text{des}}/a_t \tag{15}$$

Thus, the desired corrections of the semimajor axis and eccentricity of the chaser are

$$\delta a = \Delta a - \Delta a_{\text{des}} \tag{16}$$

$$\delta e = |\Delta e| - |\Delta e|_{\text{des}} \tag{17}$$

Gauss's perturbation equations of the semimajor axis and eccentricity are written as (see [36]),

$$\mathrm{d}\,a/\mathrm{d}t = 2a^2 v f_t/\mu \tag{18}$$

$$\mathrm{d}\,e/\mathrm{d}t = [2a(e + \cos\theta)f_t - r\sin\theta f_n]/(av) \tag{19}$$

Equation (18) shows that only f_t has an effect on the semimajor axis adjustment, but f_n does not. According to Eq. (19), it is evident that the coupling of semimajor axis and eccentricity adjustments is the weakest and f_n is the most effective to adjust eccentricity when the true anomaly θ is equal to $k\pi/2$ ($k = \pm1, \pm3, \pm5, \ldots$).

The perturbation acceleration in the LVLH frame is defined as

$$\boldsymbol{f} = \begin{bmatrix} f_x & f_y & f_z \end{bmatrix}^T \tag{20}$$

In the case of a near-circular orbit, f_t and f_n are approximately along the X and Z axes. Therefore,

$$f_t \approx f_x \tag{21}$$

$$f_n \approx f_z \tag{22}$$

Substituting Eqs. (21) and (22) into Eqs. (18) and (19) and ignoring terms containing eccentricity, Eqs. (18) and (19) become at $\theta = k\pi/2$ as follows:

$$\mathrm{d}a/\mathrm{d}t = 2\sqrt{a^3/\mu} f_x \tag{23}$$

$$\mathrm{d}\,e/\mathrm{d}t = -\sqrt{a/\mu}\sin(k\pi/2) f_z \tag{24}$$

In terms of Eq. (23), the along-track impulse Δv_x^a required to adjust the semimajor axis of the chaser by δa is

$$\Delta v_x^a = \delta a \sqrt{\mu \Big/ \left(4a_c^3\right)} \tag{25}$$

In terms of Eq. (24), the magnitude of the radial impulse Δv_z^e required to adjust the eccentricity of the chaser by δe is

$$|\Delta v_z^e| = |\delta e|\sqrt{\mu/a_c} \tag{26}$$

The sign of Δv_z^e is determined by δe and the radial relative velocity $\dot{z}$ at the time of the radial impulse. Thus, the radial impulse Δv_z^e required to adjust the eccentricity of the chaser is given by

$$\Delta v_z^e = \mathrm{sgn}(\dot{z}\delta e)|\delta e|\sqrt{\mu/a_c} \tag{27}$$

In Eqs. (25) and (27), a_c can be replaced by the semimajor axis a_t of the target with the assumption of a small difference in the semimajor axis. Thus, the impulsive velocity changes required to adjust the semimajor axis and the eccentricity of the chaser are finally written as

$$\Delta v_x^a = \delta a \sqrt{\mu \Big/ \left(4a_t^3\right)} \tag{28}$$

$$\Delta v_z^e = \mathrm{sgn}(\dot{z}\delta e)|\delta e|\sqrt{\mu/a_t} \tag{29}$$

Impulsive changes expressed by Eqs. (28) and (29) are at $\theta_c = k\pi/2$ ($k = \pm1, \pm3, \pm5, \ldots$). However the real-time true anomaly θ_c cannot be directly observed because the inertial measurements are not available. Fortunately, some special points of the target mean anomaly can be estimated using the relative position and the relative velocity. According to Eq. (7c), the radial motion z reaches the maximum $z_{\max}$ or the minimum $z_{\min}$ when M_t is equal to $n\pi$ ($n = 0, \pm1, \pm2, \pm3, \ldots$). After passing though $P_t/4$ from these extreme points, the mean anomaly of the target reaches $k\pi/2$. Meanwhile, the true anomaly of the chaser is approximately equal to $k\pi/2$ with the assumption of small eccentricity and small mean anomaly differences. Therefore, impulsive changes written by Eq. (28) and (29) will be implemented at $M_t = k\pi/2$ ($k = \pm1, \pm3, \pm5, \ldots$).

Summarizing the preceding processes, the approaches to adjust semimajor axis and eccentricity are given as follows:

Step 1) Choose the time t, determine $x(t)$ and $x(t + P_t)$, and calculate the semimajor axis difference Δa through Eq. (12).

Step 2) Determine the desired correction δa of the semimajor axis through Eq. (16), calculate the along-track impulse Δv_x^a required to adjust the semimajor axis through Eq. (28), and perform Δv_x^a when M_t reaches $k\pi/2$ for the first time after $t + P_t$.

Step 3) Determine $z_{\max}$ and $z_{\min}$ in the next orbit period after performing Δv_x^a, and calculate the magnitude of the eccentricity difference $|\Delta e|$ through Eq. (13).

Step 4) Determine the desired correction of eccentricity δe through Eq. (17), calculate the radial impulse Δv_z^e required to adjust the

eccentricity through Eq. (29), and perform Δv_z^e when M_t reaches $k\pi/2$ for the first time after determining $z_{\max}$ and $z_{\min}$.

Cross-Track Control Strategies

For many autonomous rendezvous applications such as docking between two spacecraft, it is necessary to eliminate the cross-track motion. According to Eq. (7b), the amplitude A_y of cross-track motion, which equals the maximum of cross-track motion y, is determined by a_t, i_t, the right-ascension-node difference $\Delta\Omega$, and the orbit-inclination difference Δi. Therefore, the way to eliminate cross-track motion is to eliminate the differences of the right ascension node and the orbit inclination. The desired values of the differences are

$$\Delta\Omega_{\text{des}} = 0 \tag{30}$$

$$\Delta i_{\text{des}} = 0 \tag{31}$$

Thus, the desired corrections of the right ascension node and orbit inclination of the chaser are

$$\delta\Omega = \Delta\Omega - \Delta\Omega_{\text{des}} = \Delta\Omega \tag{32}$$

$$\delta i = \Delta i - \Delta i_{\text{des}} = \Delta i \tag{33}$$

In terms of Eq. (7b), the amplitude A_y of cross-track motion is written as

$$A_y = a_t\sqrt{\Delta\Omega^2\sin^2 i_t + \Delta i^2} = a_t\sqrt{\delta\Omega^2\sin^2 i_t + \delta i^2} \tag{34}$$

Gauss's perturbation equations of the right ascension node and the orbit inclination are written as (see [36])

$$\mathrm{d}\Omega/\mathrm{d}t = r\sin u f_h/(h\sin i) \tag{35}$$

$$\mathrm{d}\,i/\mathrm{d}t = r\cos u f_h/h \tag{36}$$

where

$$h = \sqrt{\mu a(1-e^2)} \tag{37}$$

and

$$f_h = -f_y \tag{38}$$

Substituting Eqs. (37) and (38) into Eqs. (35) and (36) and ignoring terms containing eccentricity, Eqs. (35) and (36) become

$$\mathrm{d}\,\Omega/\mathrm{d}t = -\sqrt{a/\mu}\sin u f_y/\sin i \tag{39}$$

$$\mathrm{d}\,i/\mathrm{d}t = -\sqrt{a/\mu}\cos u f_y \tag{40}$$

According to Eq. (39), the cross-track impulse Δv_y^Ω required to adjust the right ascension node of the chaser by $\delta\Omega$ is

$$\Delta v_y^\Omega = -\sqrt{\mu/a_c}\sin i_c\delta\Omega/\sin u_c \tag{41}$$

According to Eq. (40), the cross-track impulse Δv_y^i required to adjust the orbit inclination of the chaser by δi is

$$\Delta v_y^i = -\sqrt{\mu/a_c}\delta i/\cos u_c \tag{42}$$

With the assumption of small orbit element differences, the orbit elements of the chaser in Eqs. (41) and (42) can be replaced by that of the target. Thus,

$$\Delta v_y^\Omega = -\sqrt{\mu/a_t}\sin i_t\delta\Omega/\sin u_t \tag{43}$$

$$\Delta v_y^i = -\sqrt{\mu/a_t}\delta i/\cos u_t \tag{44}$$

The obvious way to eliminate cross-track motion (i.e. make the chaser and target coplanar) with only one impulse is to make the impulse at the intersection points of the two orbits. Therefore, we can obtain

$$\Delta v_y = \Delta v_y^\Omega = \Delta v_y^i \tag{45}$$

Thus, the magnitude of the cross-track impulse change Δv_y is expressed as

$$|\Delta v_y| = \sqrt{\mu\left(\sin^2 i_t\delta\Omega^2 + \delta i^2\right)\Big/ a_t} = A_y\sqrt{\mu/a_t^3} \tag{46}$$

and in terms of the target argument of latitude, the location of the cross-track impulse is given by

$$u_t = \arctan 2(\sin i_t\delta\Omega, \delta i) \quad \text{or} \quad \arctan 2(-\sin i_t\delta\Omega, -\delta i) \tag{47}$$

Substituting Eq. (47) into Eq. (7b), we find $y = 0$ to be the point at which the cross-track impulsive Δv_y takes place. The sign of Δv_y is determined by the cross-track relative velocity $\dot{y}$ at the time of the cross-track impulse, which is positive at $\beta - u_t = 0$ and negative at $\beta - u_t = \pi$. Thus, the cross-track impulse Δv_y required to adjust the right ascension node and the orbit inclination of the chaser is given by

$$\Delta v_y = \mathrm{sgn}(\dot{y})A_y\sqrt{\mu/a_t^3} \tag{48}$$

Relative Navigation

The relative position and the relative velocity can be estimated when the relative range and LOS angles are measured in the chaser LVLH frame. Based on C-W equations [7], the process noise model is given by

$$\ddot{x} - 2\varpi_c\dot{z} = f_x + \varsigma_x \tag{49a}$$

$$\ddot{y} + \varpi_c^2 y = f_y + \varsigma_y \tag{49b}$$

$$\ddot{z} + 2\varpi_c\dot{x} - 3\varpi_c^2 z = f_z + \varsigma_z \tag{49c}$$

where ϖ_c can be replaced by $\sqrt{\mu/a_t^3}$ with the assumption of near-circular orbit and small differences in the semimajor axis, and ς_x, ς_y, and ς_z are the random accelerations acting on the chaser, which are assumed to be white noises with the following characteristics:

$$\begin{gathered} E(\varsigma_x^2) = \sigma_{px}^2\delta(t-\tau), \qquad E(\varsigma_y^2) = \sigma_{py}^2\delta(t-\tau) \\ E(\varsigma_z^2) = \sigma_{pz}^2\delta(t-\tau) \end{gathered} \tag{50}$$

where σ_{px}, σ_{py}, and σ_{pz} are the standard deviations of the process noise accelerations, and δ denotes the Dirac delta operator.

The measurement model is given by

$$r = \sqrt{x^2 + y^2 + z^2} + \nu_r \tag{51a}$$

$$\theta_y = \arctan 2(-z, x) + \nu_y \tag{51b}$$

$$\theta_z = \arctan(y, \sqrt{x^2 + z^2}) + \nu_z \tag{51c}$$

where θ_y and θ_z are LOS angles that are explained in the next section (see Fig. 2), and ν_y and ν_z are LOS angles measurement noises. These noises are assumed to be white, with the expected value to be zero and the standard deviations to be σ_r, σ_y, and σ_z, respectively.

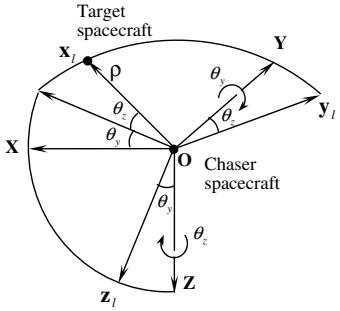

Fig. 2 Scenario 1: LOS frame centered on the center of mass of the chaser spacecraft.

Based on the process noise model Eq. (49) and the measurements model Eq. (51), an EKF is designed to estimate the relative position and the relative velocity [5,37].

Along-Track Motion Control Using Only Azimuth Angle

This section investigates along-track motion control using only LOS angles. When the lidar (providing relative range measurements) is invalid, the only acquirable measurements are LOS angles. In this case, it is difficult to estimate the relative position and the relative velocity using filter algorithms. Especially when the relative range is large, the estimation error is so great that the relative motion cannot be controlled accurately. Therefore, we present an iterative algorithm to estimate the along-track motion and obtain the impulsive changes to adjust it using only azimuth angle measurement.

LOS Frame and LOS Angles

Figure 2 depicts the LOS angles and LOS frame centered on the center of mass of the chaser spacecraft. The chaser LVLH frame $OXYZ$ rotates about the Y axis through angle θ_y and then rotates about the Z axis through angle θ_z to become LOS frame $Ox_l y_l z_l$. The x_l axis of the LOS frame is in alignment with the relative position vector of the target with respect to the chaser $\boldsymbol{\rho}$. Therefore, LOS angles θ_y (azimuth) and θ_z (elevation), measured from the chaser LVLH frame, are related to the components $[x\ y\ z]^T$ of the relative vector $\boldsymbol{\rho}$ as follows:

$$\theta_y = \arctan 2(-z, x), \qquad \theta_y \in [-\pi, \pi] \tag{52}$$

$$\theta_z = \arctan(y, \sqrt{x^2 + z^2}), \qquad \theta_z \in [-\pi/2, \pi/2] \tag{53}$$

In terms of the sign of along-track motion x, Eq. (52) is rewritten as

$$\theta_y = \begin{cases} \arctan(-z/x) & x > 0 \\ \arctan(-z/x) + \pi & x < 0 \end{cases} \tag{54}$$

Equation (54) presents two forms to calculate azimuth θ_y for different signs of along-track motion x. Because the target is always ahead of or behind the chaser during the whole relative drift phase, the along-track motion x is either above zero or below zero all the time. Therefore, only one of two forms of Eq. (54) will be required to calculate the azimuth angle θ_y.

Along-Track Motion Estimate and Control

Azimuth angles at $t, t + P_t, t + 2P_t$, and $t + 3P_t$ time are defined as $\theta_y(t)$, $\theta_y(t + P_t)$, $\theta_y(t + 2P_t)$, and $\theta_y(t + 3P_t)$. Note that the nominal semimajor axis a_t of the target is still required and the period P_t of the target is calculated with $2\pi\sqrt{a_t^3/\mu}$. According to Eq. (54), the varying of the azimuth angle θ_y within one orbit period P_t is expressed as (with reference to Fig. 3)

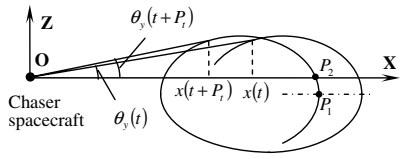

Fig. 3 Scenario 1: azimuth angle and relative motion in the orbital plane.

$$\theta_y(t + P_t) - \theta_y(t) = \arctan[-z(t + P_t)/x(t + P_t)] - \arctan[-z(t)/x(t)] \tag{55}$$

A Taylor's series expansion of $\arctan[-z(t + P_t)/x(t + P_t)]$ in the neighborhood of point $[x(t), z(t)]$, first-order terms retained, leads to

$$\theta_y(t + P_t) - \theta_y(t) = -\frac{\tan\theta_y(t)[x(t + P_t) - x(t)] + [z(t + P_t) - z(t)]}{x(t)[1 + \tan^2\theta_y(t)]} \tag{56}$$

When unperturbed, the orbit radial motion z is periodic motion, with the period equal to the orbit period P_t of the target. Then

$$z(t + P_t) - z(t) = 0 \tag{57}$$

Substituting Eq. (57) into Eq. (56) and transforming Eq. (56) yields

$$x(t + P_t) - x(t) = -\frac{x(t)[\theta_y(t + P_t) - \theta_y(t)][1 + \tan^2\theta_y(t)]}{\tan\theta_y(t)} \tag{58}$$

The only quantity on the right-hand side of Eq. (58) that is not directly measurable is the along-track motion $x(t)$. Therefore, when $x^{(0)}$ is given as the initial guess of $x(t)$ and Eqs. (12) and (58) are used, the initial estimate of the semimajor axis difference within the orbit period $[t, t + P_t]$ is expressed as

$$\Delta a_1^{(0)} = \frac{x^{(0)}[\theta_y(t + P_t) - \theta_y(t)][1 + \tan^2\theta_y(t)]}{3\pi\tan\theta_y(t)} \tag{59}$$

Then, based on the desired value Δa_{des} of the semimajor axis difference and Eq. (16), the first desired correction of the semimajor axis of the chaser is written as

$$\delta a_1 = \Delta a_1^{(0)} - \Delta a_{\text{des}} \tag{60}$$

According to Eq. (28), the first along-track impulse required to adjust the semimajor axis of the chaser is obtained as

$$\Delta v_{x1}^a = \delta a_1\sqrt{\mu/(4a_t^3)} \tag{61}$$

To have as little effect as possible on eccentricity, it is best that the along-track impulse Δv_{x1}^a takes place at $\theta_c = k\pi/2$ ($k = \pm 1, \pm 3, \pm 5, \ldots$) (approximately the point P_1 in Fig. 3). However, the point P_1 cannot be determined by measurement. Therefore the point P_2, which can be determined when the azimuth angle θ_y arrives at zero for the first time after $t + P_t$, is chosen as the position at which the along-track impulse Δv_{x1}^a is implemented.

The preceding process presents the first along-track impulsive velocity change required to adjust the semimajor axis difference. However, the semimajor axis difference cannot reach the desired value with only the first along-track impulse, because the initial guess $x^{(0)}$ of the relative motion at the time t is inaccurate and the resolving process of control strategy involves approximation steps. Thus, it is necessary to implement one more correction maneuver.

Similar to Eq. (59), the initial estimate of the semimajor axis difference within the orbit period $[t + 2P_t, t + 3P_t]$ after the first impulsive velocity change is expressed as

$$\Delta a_2^{(0)} = \frac{x(t+2P_t)[\theta_y(t+3P_t)-\theta_y(t+2P_t)][1+\tan^2\theta_y(t+2P_t)]}{3\pi\tan\theta_y(t+2P_t)} \tag{62}$$

where $x(t+2P_t)$ is estimated by $x^{(0)}$, $\Delta a_1^{(0)}$, δa_1, and the time t_{P_2} of the first along-track impulse at the point P_2. The estimated along-track motion is drifting with the semimajor axis difference $\Delta a_1^{(0)}$ before t_{P_2} and then with the semimajor axis difference $\Delta a_1^{(0)} - \delta a_1$ after t_{P_2}. Thus, $x(t+2P_t)$ is expressed as follows:

$$x(t+2P_t) = x^{(0)} - 3\pi\frac{(t_{P_2}-t)}{P_t}\Delta a_1^{(0)} - 3\pi\frac{(t+2P_t-t_{P_2})}{P_t}(\Delta a_1^{(0)} - \delta a_1) \tag{63}$$

It is inevitable that the estimate value $\Delta a_2^{(0)}$ from Eq. (62) is not equal to the desired value Δa_{des}, strictly because of the inaccurate initial guess of the relative motion and the approximate steps. Therefore, when the estimate value $\Delta a_2^{(0)}$ and the first correction δa_1 of the semimajor axis are used, the second estimate of the semimajor axis difference with the orbit period $[t, t+P_t]$ is obtained:

$$\Delta a_1^{(1)} = \Delta a_2^{(0)} + \delta a_1 \tag{64}$$

And then, by substituting $\Delta a_1^{(1)}$ into the left-hand side of Eq. (59), the first estimate $x^{(1)}$ of the relative motion at the time t is calculated with Eq. (59). Through substituting the new estimates $\Delta a_1^{(1)}$ and $x^{(1)}$ into Eqs. (62) and (63), the second estimate $\Delta a_2^{(1)}$ of the semimajor axis difference within the orbit period $[t+2P_t, t+3P_t]$ can be obtained. Thus, according to the preceding process, the iterative algorithm is given by

$$\Delta a_1^{(k)} = \frac{x^{(k)}[\theta_y(t+P_t)-\theta_y(t)][1+\tan^2\theta_y(t)]}{3\pi\tan\theta_y(t)} \tag{65a}$$

$$\Delta a_2^{(k)} = \frac{x(t+2P_t)[\theta_y(t+3P_t)-\theta_y(t+2P_t)][1+\tan^2\theta_y(t+2P_t)]}{3\pi\tan\theta_y(t+2P_t)} \tag{65b}$$

$$x(t+2P_t) = x^{(k)} - 3\pi\frac{(t_{P_2}-t)}{P_t}\Delta a_1^{(k)} - 3\pi\frac{(t+2P_t-t_{P_2})}{P_t}(\Delta a_1^{(k)} - \delta a_1) \tag{65c}$$

$$\delta a_1 = \Delta a_1^{(0)} - \Delta a_{\text{exp}} \tag{65d}$$

$$\Delta a_1^{(k+1)} = \Delta a_2^{(k)} + \delta a_1, \qquad k = 0, 1, 2, \ldots \tag{65e}$$

When the iterative value is sufficiently precise, namely,

$$|\Delta a_2^{(k+1)} - \Delta a_2^{(k)}| \le \Delta \tag{66}$$

where Δ is the error limit of the estimate value of the semimajor axis difference, the iterative process is stopped. The convergence of the iterative algorithm is analyzed in the Appendix.

The second desired correction of the semimajor axis of the chaser is written as

$$\delta a_2 = \Delta a_2^{(k+1)} - \Delta a_{\text{des}} \tag{67}$$

and the second along-track impulsive velocity change required to adjust the semimajor axis of the chaser is given by

$$\Delta v_{x2}^a = \delta a_2\sqrt{\mu\Big/\left(4a_t^3\right)} \tag{68}$$

It takes place at the time when the azimuth angle θ_y arrives at zero for the first time after $t + 3P_t$.

In fact, the semimajor axis difference is not equal to the desired value Δa_{des} precisely after the second along-track impulsive velocity change. To improve the precision of the semimajor axis difference, additional along-track impulses can be designed using the preceding iterative algorithm. In addition, it is difficult to control the radial motion and the cross-track motion precisely, because their extreme values cannot be determined by only LOS angles. These problems will be studied in the future.

Numerical Simulations

The preceding control strategies are illustrated now by two scenarios, first with relative position and velocity available and then with only LOS angles available. The initial classical orbit elements of the target are given in Table 1. The target is assumed to be flying at a 7000-km near-circular orbit with small eccentricity. The initial orbit element differences are given in Table 2. The initial semimajor axis difference is different in two scenarios.

Using the initial orbit elements of the target and the chaser, we can calculate the initial inertial positions and velocities of the two spacecraft, which are taken as the initial values for numerical integration. And then, using a standard fourth-order Runge–Kutta method with a fixed step of 0.2 s, the numerical simulations are performed by integrating the nonlinear orbit equations (Cowell's method [36])

$$\ddot{\boldsymbol{r}}_t = -\mu\boldsymbol{r}_t/r_t^3 + \boldsymbol{f}(\boldsymbol{r}_t) \tag{69}$$

$$\ddot{\boldsymbol{r}}_c = -\mu\boldsymbol{r}_c/r_c^3 + \boldsymbol{f}(\boldsymbol{r}_c) \tag{70}$$

where the target's perturbation acceleration $\boldsymbol{f}(\boldsymbol{r}_t)$ includes the gravitational zonal J_2 through J_4 effects, and the chaser's perturbation acceleration $\boldsymbol{f}(\boldsymbol{r}_c)$ includes the gravitational zonal J_2 through J_4 effects and the control impulsive changes. All calculations are carried out with Matlab M-file programs and Simulink models.

Table 1 Target's initial orbit elements

Orbit elements	Value
a_t, m	7,000,000
e_t	0.002
i_t, deg	50.0
Ω_t, deg	10.0
ω_t, deg	30.0
M_t, deg	110.0

Table 2 Initial orbit element differences

Orbit elements	Value
Δa, m	Scenario 1: 300 scenario 2: 1500
Δe	−0.0006
Δi, deg	−0.0050
$\Delta\Omega$, deg	−0.0050
$\Delta\omega$, deg	0.2500
ΔM, deg	0.3000

Table 3 Relative navigation parameters

Parameters		Value
Standard deviations of process acceleration noises	σ_{px}, m/s^2	0.003
	σ_{py}, m/s^2	0.00005
	σ_{pz}, m/s^2	0.004
Standard deviations of measurement noises	σ_r, m	16.67
	σ_y, deg	0.01
	σ_z, deg	0.01
Initial estimation of state vector $[\hat{x}, \hat{y}, \hat{z}, \hat{\dot{x}}, \hat{\dot{y}}, \hat{\dot{z}}]^T$		$[70\text{ km}, 0, 0, 0, 0, 0]^T$
Initial covariance matrix $\boldsymbol{P}_0$		diag[100 m^2, 100 m^2, 100 m^2, 10 (m/s)^2, 10 (m/s)^2, 10 (m/s)^2]

Scenario 1: Relative Motion Control Using Relative Position and Velocity Estimations

In this scenario, we show an example of approach operation using the relative position and velocity, which are estimated by EKF with the relative range and LOS angle measurements. The relative navigation parameters are presented in Table 3.

In the beginning, the chaser lags behind the target and is expected to approach it with a 10-km along-track drift per orbit period. Then, as long as the along-track range decreases to below 10 km, the along-track drift is expected to be eliminated (namely, $\Delta a_{\text{des}} = 10\text{ km}/3\pi \rightarrow 0$) and the oscillatory amplitude of radial motion is designed to be adjusted to 1 km (namely, $A_z^{\text{des}} = 1\text{ km}$). Furthermore, the cross-track motion also needs to be eliminated. The simulation is done for 50,000 s ($\approx$8.5785 target orbit period).

Three-axis impulses are shown in Table 4. Figure 4 shows that the semimajor axis difference rises from 300 to 1064 m after the first along-track impulse, and then decreases from 1064 to 2 m after the second along-track impulse. However, after the radial impulse is performed, the decreased semimajor axis difference rises again to about 18.5 m, because the radial impulse causes a little acceleration component along the velocity direction for the near-circular orbit case. Furthermore, the drift of along-track motion decreases from -2805.3 m (D_1 in Fig. 5) per orbit to $-10,016.1$ m (D_2 in Fig. 5) per orbit and finally increases to -174.0 m per orbit (D_3 in Fig. 5). The results also illustrate that the drift of along-track motion is -3π times as much as the corresponding semimajor axis difference. Figure 6 displays that the radial impulse results in the magnitude of eccentricity difference decreasing. The magnitude of radial motion decreases from 4345.9 m (A_{z1} in Fig. 7) to 995.5 m (A_{z2} in Fig. 7). Figure 8 shows that the initial magnitude of cross-track motion is 728.8 m (A_{y1}) and then decreases to 2.1 m (A_{y2}) after the cross-track impulse. Figures 9–11 are the relative orbits in the chaser LVLH frame that satisfy the desired requirement. Figure 12 is the relative position estimation errors with the accuracy of less than 10 m. Figure 13 is the relative velocity estimation errors with the accuracy of less than 0.2 m/s. The jumps of estimation errors in Figs. 12 and 13 attribute to the control impulses.

Scenario 2: Along-Track Motion Control Using Only Azimuth Angle Measurement

In this scenario, one example of along-track drift control using only azimuth angle measurement is provided. The standard deviation of angle measurement noise is $\sigma_y = 0.01$ deg. The chaser is designed to approach the target with a 5-km along-track drift per orbit period and to stop approaching as long as the along-track range decreases to below 20 km (namely, $\Delta a_{\text{des}} = 5\text{ km}/3\pi \rightarrow 0$). The initial guess of along-track motion is $x^{(0)} = 50$ km. The simulation is done for 60,000 s ($\approx$10.2942 target orbit period).

Table 5 presents four along-track impulses. Figure 14 shows that the semimajor axis difference decreases from 1500 to 669 m after the

Table 4 Three-axis impulsive velocity changes

Impulsive changes		Value, m/s	Performing time, s
Along-track Δv_x^a	First	-0.41206	8474.6
	Second	0.57241	34,809.8
Cross-track Δv_y		0.78557	39,038.2
Radial Δv_z^e		3.60682	40,862.8
Total velocity increment, m/s		5.37686	

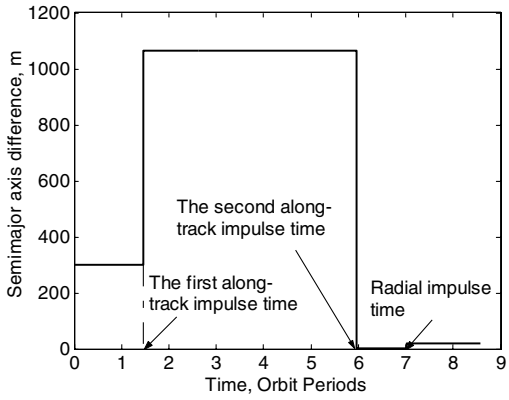

Fig. 4 Scenario 1: semimajor axis difference vs time.

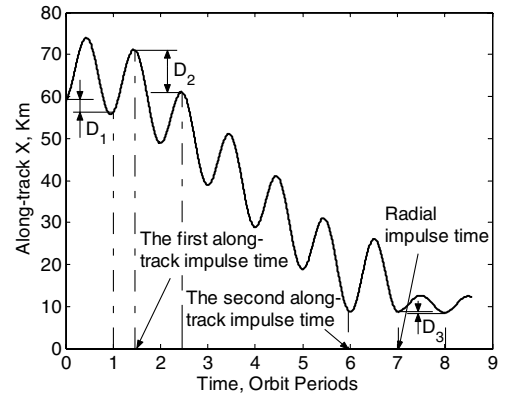

Fig. 5 Scenario 1: along-track motion x vs time.

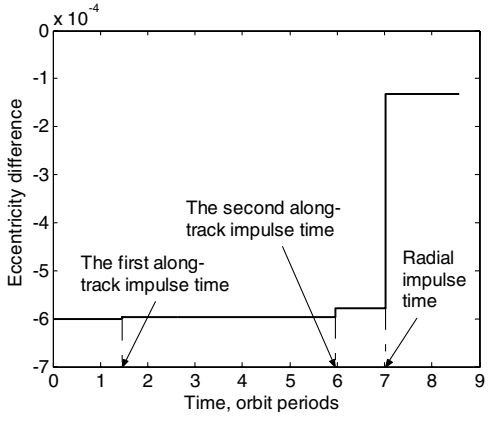

Fig. 6 Scenario 1: eccentricity difference vs time.

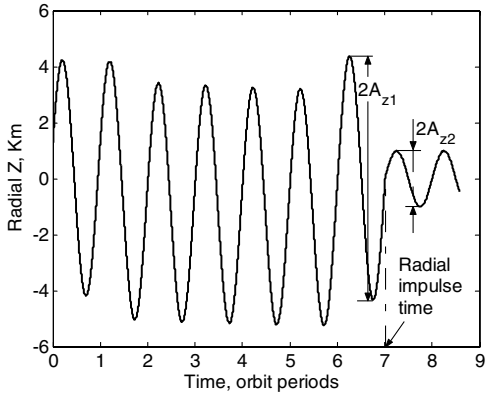

Fig. 7 Scenario 1: radial motion z vs time.

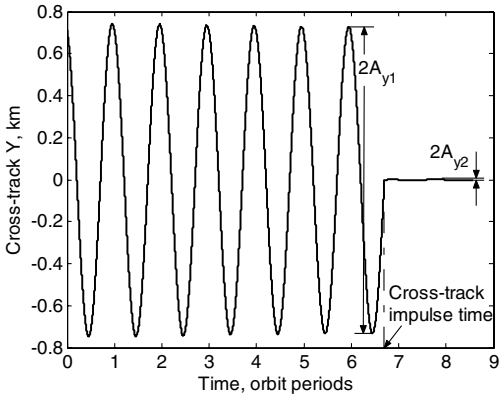

Fig. 8 Scenario 1: cross-track motion y vs time.

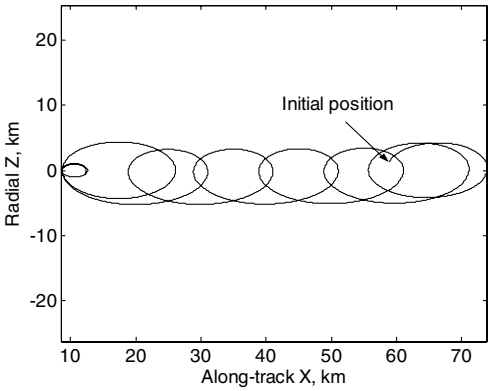

Fig. 9 Scenario 1: relative orbit in the X–Z plane (the chaser LVLH).

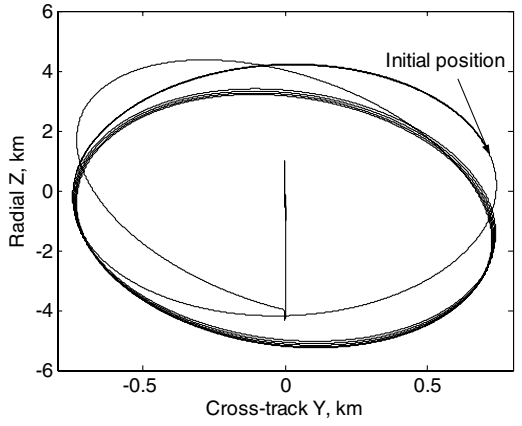

Fig. 10 Scenario 1: relative orbit in the Y–Z plane (the chaser LVLH).

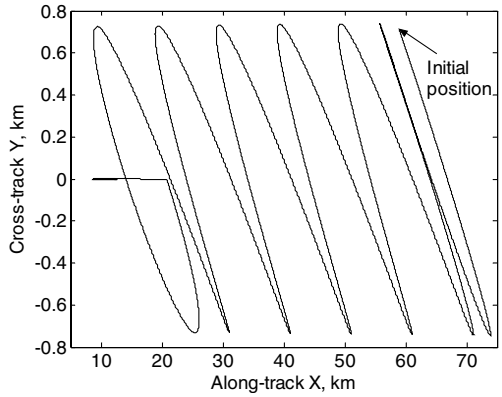

Fig. 11 Scenario 1: relative orbit in the X–Y plane (the chaser LVLH).

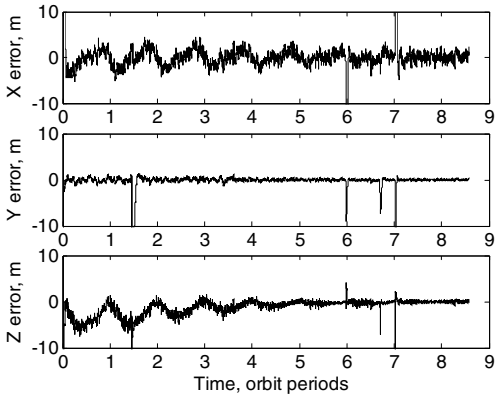

Fig. 12 Scenario 1: relative position estimation errors.

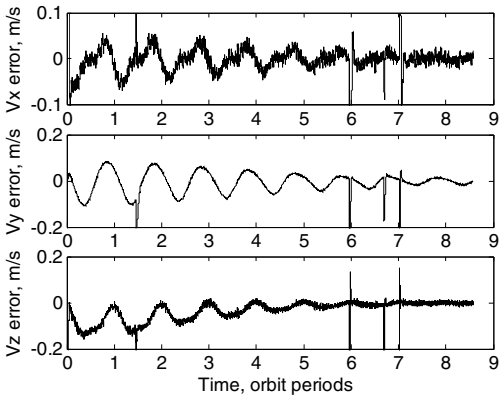

Fig. 13 Scenario 1: relative velocity estimation errors.

first and second along-track impulses. Accordingly, the drift of along-track motion increases from $-14,110.4$ m per orbit (D_1 in Fig. 15) to -6286.1 m (D_2 in Fig. 15) per orbit. The drift velocity of the along-track motion does not reach the desired value of 5 km because of azimuth measurement error. The semimajor axis difference finally decreases to 12.7 m after the third and fourth along-track impulses and the drift of along-track motion increases to

Table 5 Along-track impulses

Along-track impulses	Value, m/s	Performing time, s
First	0.42422	8141.0
Second	0.02415	19767.8
Third	0.23720	31,401.2
Fourth	0.11711	43,050.6
Total velocity increment, m/s	0.80268	

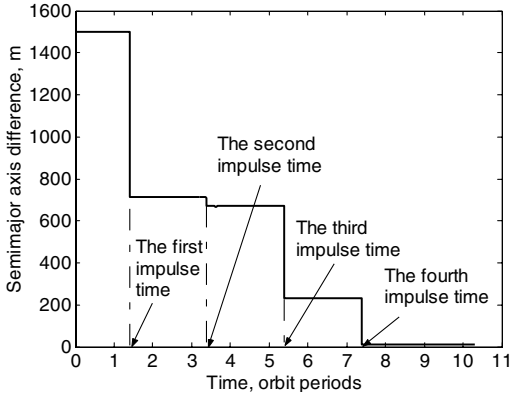

Fig. 14 Scenario 2: semimajor axis difference vs time.

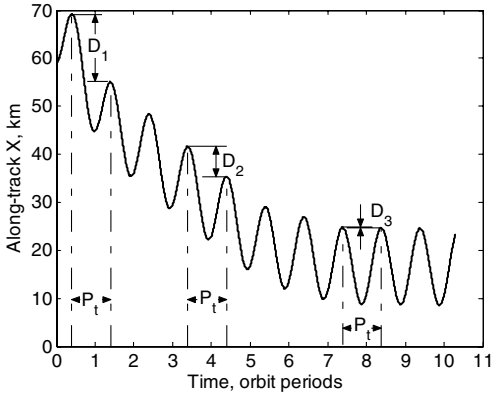

Fig. 15 Scenario 2: along-track motion x vs time.

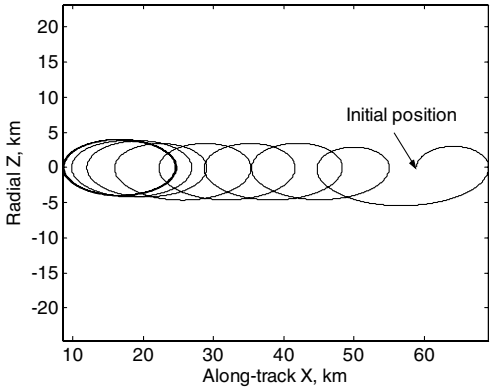

Fig. 16 Scenario 2: relative orbit in the X–Z plane (the chaser LVLH).

-101.2 m per orbit (D_3 in Fig. 15). As seen in Fig. 16, the relative orbit in the X–Z plane tends to be stabilized. Figure 17 shows the azimuth angle and the measurement error.

The results indicate that the control errors are inevitable. But in the long-range (several tens of kilometers) drift phase of autonomous rendezvous, the order of these errors is acceptable. Therefore, the iterative algorithm is valid for drift control of autonomous rendezvous with only LOS angles available.

Conclusions

According to the periodic characteristics of relative motion described by classic orbit element differences, impulse algorithms are developed and illustrated for relative motion control in two different measurement cases. In the first case, the measurements of relative range and LOS angles are available. The relative position and the relative velocity are estimated to determine the semimajor axis difference, the magnitude of eccentricity difference, and the amplitude of cross-track motion. The impulsive control strategies designed with Gauss's perturbation equations are efficient for adjusting the along-track drift and the amplitudes of radial and cross-track motion. In the second case, only LOS angles are available. The relation between the azimuth angle and the semimajor axis difference is established and used to design along-track impulses that are efficient to control the along-track drift. The proposed control strategies are verified by the numerical simulations of relative motion maneuver for example scenarios. The results indicate that

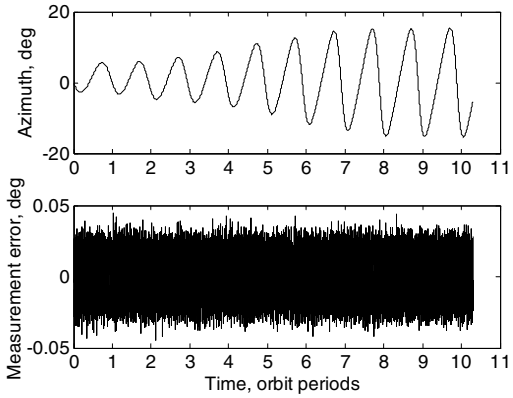

Fig. 17 Scenario 2: azimuth angle vs time.

1) Along-track, radial, and cross-track motions can be controlled accurately when the relative range and LOS angles are available.

2) The iterative algorithm is valid for along-track drift control when only LOS angles are available.

The proposed control strategies have three advantages:

1) Only relative measurements are required.

2) The strategies are suited to the long-range relative motion.

3) The algorithms are simple for autonomous application. They will be helpful for maneuver operations in the relative drift phase of autonomous rendezvous, especially in noncooperation cases that lack measurements.

However, the control strategies are applied only to the case of near-circular orbits, and the iterative algorithms using only LOS angles are not suitable for all autonomous rendezvous operations. The case of elliptical orbits and the radial and cross-track maneuver strategies using only LOS angles need to be studied in the future.

Appendix: Convergence of the Iterative Algorithm

Using Eqs. (65a–65e), the series $\Delta a_2^{(k)}$ is expressed as follows:

$$\Delta a_2^{(k)} = \left\{\frac{\tan\theta_y(t)}{[\theta_y(t+P_t)-\theta_y(t)][1+\tan^2\theta_y(t)]} - 2\right\} \cdot \frac{[\theta_y(t+3P_t)-\theta_y(t+2P_t)][1+\tan^2\theta_y(t+2P_t)]}{\tan\theta_y(t+2P_t)} \Delta a_2^{(k-1)} + \left\{\frac{\tan\theta_y(t)}{[\theta_y(t+P_t)-\theta_y(t)][1+\tan^2\theta_y(t)]} + \frac{t-t_{P_2}}{P_t}\right\} \cdot \frac{[\theta_y(t+3P_t)-\theta_y(t+2P_t)][1+\tan^2\theta_y(t+2P_t)]}{\tan\theta_y(t+2P_t)} \delta a_1 \tag{A1}$$

defining

$$B = \left\{\frac{\tan\theta_y(t)}{[\theta_y(t+P_t)-\theta_y(t)][1+\tan^2\theta_y(t)]} - 2\right\} \times \frac{[\theta_y(t+3P_t)-\theta_y(t+2P_t)][1+\tan^2\theta_y(t+2P_t)]}{\tan\theta_y(t+2P_t)} \tag{A2}$$

$$C = \left\{ \frac{\tan\theta_y(t)}{[\theta_y(t+P_t)-\theta_y(t)][1+\tan^2\theta_y(t)]} + \frac{t-t_{P_2}}{P_t} \right\} \times \frac{[\theta_y(t+3P_t)-\theta_y(t+2P_t)][1+\tan^2\theta_y(t+2P_t)]}{\tan\theta_y(t+2P_t)} \tag{A3}$$

then

$$\Delta a_2^{(k)} = B\Delta a_2^{(k-1)} + C\delta a_1 = B^{k-1}\Delta a_2^{(1)} + (B^{k-2} + B^{k-3} + \cdots + B + 1)C\delta a_1 = B^{k-1}\Delta a_2^{(1)} + \frac{1-B^{k-1}}{1-B}C\delta a_1 \tag{A4}$$

Apparently from the preceding equation, the convergence condition of the iterative algorithm is $|B| < 1$. Using Eqs. (12) and (58), B is simplified as follows:

$$B = \left[\frac{x(t)}{x(t+P_t)-x(t)} - 2\right]\frac{x(t+3P_t)-x(t+2P_t)}{x(t+2P_t)} = \frac{\Delta a_2[x(t)-6\pi\Delta a_1]}{\Delta a_1 x(t+2P_t)} \tag{A5}$$

where Δa_1 is the initial semimajor axis difference within the orbit period $[t, t+P_t]$ and Δa_2 is the semimajor axis difference within the orbit period $[t+2P_t, t+3P_t]$ after the first along-track impulse; $x(t+2P_t)$ can be replaced by Eq. (63). Thus, the sufficient condition of convergence is

$$|\Delta a_2[x(t)-6\pi\Delta a_1]| < |\Delta a_1 x(t+2P_t)| \tag{A6}$$

We will subsequently analyze the convergent conditions for different rendezvous operations.

When the chaser approaches the target in the beginning, namely,

$$x(t)\Delta a_1 > 0 \tag{A7}$$

and the approach velocity is excepted to decrease, namely,

$$|\Delta a_{\text{des}}| < |\Delta a_1| \tag{A8}$$

$|\Delta a_2| < |\Delta a_1|$ and $|x(t)-6\pi\Delta a_1| < |x(t+2P_t)|$ can be derived. Therefore, Eq. (A6) is satisfied and the iterative algorithm is convergent.

When the chaser retreats from the target in the beginning, namely,

$$x(t)\Delta a_1 < 0 \tag{A9}$$

and the retreat velocity is excepted to decrease, $|\Delta a_2| < |\Delta a_1|$ and $|x(t)-6\pi\Delta a_1| > |x(t+2P_t)|$ can be derived. Equation (A6) is not always satisfied. But if magnitude of the initial along-track drift per orbit period is small in comparison with the along-track range (namely, $|3\pi\Delta a_1| \ll |x(t)|$), we have $|x(t)-6\pi\Delta a_1| \approx |x(t+2P_t)|$ and Eq. (A6) is satisfied. The iterative algorithm is convergent.

When the drift velocity is expected to increase, namely,

$$|\Delta a_{\text{des}}| > |\Delta a_1| \tag{A10}$$

the iterative algorithm cannot converge, whether for approach or for retirement.

References

[1] Polites, M. E., "An Assessment of the Technology of Automated Rendezvous and Capture in Space," NASA TP1998-208528, 1998.

[2] Wertz, J. R., and Bell, R., "Autonomous Rendezvous and Docking Technologies—Status and Prospects," Space Systems Technology and Operations Conference, Orlando, FL, SPIE—International Society for Optical Engineering, Paper 5088-3, 2003.

[3] Zimpfer, D., Kachmar, P., and Tuohy, S., "Autonomous Rendezvous, Capture and In-Space Assembly: Past, Present and Future," 1st Space Exploration Conference: Continuing the Voyage of Discovery, Orlando FL, AIAA Paper 2005-2523, 2005.

[4] Machula, M. F., and Sandhoo, G. S., "Rendezvous and Docking for Space Exploration," 1st Space Exploration Conference: Continuing the Voyage of Discovery, Orlando FL, AIAA Paper 2005-2716, 2005.

[5] Hablani, H. B., Tapper, M. L., and Dana-Bashian, D. J., "Guidance and Relative Navigation for Autonomous Rendezvous in a Circular Orbit," *Journal of Guidance, Control, and Dynamics*, Vol. 25, No. 3, 2002, pp. 553–562.

[6] Hablani, H. B., "Autonomous Relative Navigation, Attitude Determination, Pointing and Tracking for Spacecraft Rendezvous," AIAA Guidance, Navigation, and Control Conference Exhibit, Austin, TX, AIAA Paper 2003-5355, 2003.

[7] Crassidis, J. L., Alonso, R., and Junkins, J. L., "Optimal Attitude and Position Determination from Line-of-Sight Measurements," *Journal of the Astronautical Sciences*, Vol. 48, Nos. 2–3, Apr.–Sept. 2000, pp. 391–408.

[8] Yim, J. R., Crassidis, J. L., and Junkins, J. L., "Autonomous Orbit Navigation of Two Spacecraft System Using Relative Line of Sight Vector Measurements," AAS/AIAA Spaceflight Mechanics Meeting, Maui, HI, American Astronautical Society Paper 04-257, Feb. 2004.

[9] Clohessy, W. H., and Wiltshire, R. S., "Terminal Guidance System for Satellite Rendezvous," *Journal of the Aerospace Sciences*, Vol. 27, No. 9, 1960, pp. 653–674.

[10] Hill, G. W., "Researches in the Lunar Theory," *American Journal of Mathematics*, Vol. 1, 1878, pp. 5–26.

[11] Fehse, W., *Automated Rendezvous and Docking of Spacecraft*, Cambridge Univ. Press, Cambridge, England, U.K., 2003, Chap. 3.

[12] Prussing, J. E., "Optimal Four-Impulse Fixed-Time Rendezvous in the Vicinity of a Circular Orbit," *AIAA Journal*, Vol. 7, No. 5, 1969, pp. 928–935.

[13] Prussing, J. E., "Optimal Two- and Three-Impulse Fixed-Time Rendezvous in the Vicinity of a Circular Orbit," *AIAA Journal*, Vol. 8, No. 7, 1970, pp. 1221–1228.

[14] Carter, T., "Fuel-Optimal Maneuvers of a Spacecraft Relative to a Point in Circular Orbit," *Journal of Guidance, Control, and Dynamics*, Vol. 7, No. 6, 1984, pp. 710–716.

[15] Lopez, I., and McInnes, C. R., "Autonomous Rendezvous Using Artificial Potential Function Guidance," *Journal of Guidance, Control, and Dynamics*, Vol. 18, No. 2, 1995, pp. 231–241.

[16] Lovell, T. A., and Tragesser, S. G., "A Practical Guidance Methodology for Relative Motion of LEO Spacecraft Based on the Clohessy-Wiltshire Equations," AAS/AIAA Spaceflight Mechanics Meeting, Maui, HI, American Astronautical Society Paper 04-252, 2004.

[17] Lovell, T. A., and Tragesser, S. G., "Guidance for Relative Motion of Low Earth Orbit Spacecraft Based on Relative Orbit Elements," AIAA/AAS Astrodynamics Specialist Conference and Exhibit, Providence, RI, AIAA Paper 2004-4988, 2004.

[18] Lawden, D. F., *Optimal Trajectories for Space Navigation*, Butterworths, London, 1963, pp. 79–86.

[19] Carter, T., Humi, M., "Fuel-Optimal Rendezvous Near a Point in General Keplerian Orbit," *Journal of Guidance, Control, and Dynamics*, Vol. 16, No. 6, 1987, pp. 567–573.

[20] Carter, T., "New Form for the Optimal Rendezvous Equations Near a Keplerian Orbit," *Journal of Guidance, Control, and Dynamics*, Vol. 13, No. 1, 1990, pp. 183–186.

[21] Carter, T., "State Transition Matrices for Terminal Rendezvous Studies: Brief Survey and New Example," *Journal of Guidance, Control, and Dynamics*, Vol. 21, No. 1, 1998, pp. 148–155.

[22] Melton, R. G., "Time-Explicit Representation of Relative Motion Between Elliptical Orbits," *Journal of Guidance, Control, and Dynamics*, Vol. 23, No. 4, 2000, pp. 604–610.

[23] Yamanaka, K., and Ankersen, F., "New State Transition Matrix for Relative Motion on an Arbitrary Elliptical Orbit," *Journal of Guidance, Control, and Dynamics*, Vol. 25, No. 1, 2002, pp. 60–66.

[24] Inalhan, G., and How, J., "Relative Dynamics and Control of Spacecraft Formations in Elliptic Orbits," *Journal of Guidance, Control, and Dynamics*, Vol. 25, No. 1, 2002, pp. 48–59.

[25] Vaddi, S. S., Vadali, S. R., and Alfriend, K. T., "Formation Flying: Accommodating Nonlinearity and Eccentricity Perturbations," *Journal of Guidance, Control, and Dynamics*, Vol. 26, No. 2, 2002, pp. 214–223.

[26] Karlgard, C. D., and Lutze, F. H., "Second Order Relative Motion Equations," *Advances in the Astronautical Sciences*, Vol. 109, No. 3, 2002, pp. 2429–2448.

[27] Mitchell, J. W., and Richardson, D. L., "A Third Order Analytical Solution for Relative Motion with a Circular Reference Orbit," *Journal of the Astronautical Sciences*, Vol. 51, No. 1, 2003, pp. 1–12.

[28] Gim, D. W., and Alfriend, K. T., "State Transition Matrix of Relative Motion for the Perturbed Noncircular Reference Orbit," *Journal of Guidance, Control, and Dynamics*, Vol. 26, No. 6, 2003, pp. 956–971.

[29] Schaub, H., and Alfriend, K. T., "J_2 Invariant Reference Orbits for Spacecraft Formations," *Celestial Mechanics and Dynamical Astronomy*, Vol. 79, No. 2, 2001, pp. 77–95.

[30] Alfriend, K. T., and Schaub, H., "Dynamic and Control of Spacecraft Formations: Challenges and Some Solutions," *Journal of the Astronautical Sciences*, Vol. 48, Nos. 2–3, 2000, pp. 249–267.

[31] Schaub, H., and Alfriend, K. T., "Hybrid Cartesian and Orbit Element Feedback Law for Formation Flying Spacecraft," *Journal of Guidance, Control, and Dynamics*, Vol. 25, No. 2, 2002, pp. 387–393.

[32] Schaub, H., "Relative Orbit Geometry through Classical Orbit Element Differences," *Journal of Guidance, Control, and Dynamics*, Vol. 27, No. 5, 2004, pp. 839–848.

[33] Schaub, H., Vadali, S. R., Junkins, J. L., and Alfriend, K. T., "Spacecraft Formation Flying Control Using Mean Orbit Elements," *Journal of the Astronautical Sciences*, Vol. 48, No. 1, 2000, pp. 69–87.

[34] Schaub, H., and Alfriend, K. T., "Impulsive Feedback Control to Establish Specific Mean Orbit Elements of Spacecraft Formations," *Journal of Guidance, Control, and Dynamics*, Vol. 24, No. 4, 2001, pp. 739–745.

[35] Schaub, H., and Junkins, J. L., *Analytical Mechanics of Space Systems*, AIAA Education Series, AIAA, Reston, VA, 2003, pp. 606–609.

[36] Battin, R. H., *An Introduction to The Mathematics and Methods of Astrodynamics*, AIAA Education Series, AIAA, New York, 1987, pp. 206–212, 447, 498.

[37] Gelb, A. (ed.), *Applied Optimal Estimation*, MIT Press, Cambridge, MA, 1974, Chap. 3.